Author/s:
Reed, WR;Dunstan, MA;Gable, RW;Phonsri, W;Murray, KS;Mole, RA;Boskovic, C

Title:
Tetraoxolene-bridged rare-earth complexes: A radical-bridged dinuclear Dy single-molecule magnet

Date:
2019-01-01

Citation:
Reed, W. R., Dunstan, M. A., Gable, R. W., Phonsri, W., Murray, K. S., Mole, R. A. & Boskovic, C. (2019). Tetraoxolene-bridged rare-earth complexes: A radical-bridged dinuclear Dy single-molecule magnet. Dalton Transactions, 48 (41), pp.15635-15645. https://doi.org/10.1039/c9dt01320b.

Tetraoxolene-bridged rare-earth complexes: a radical-bridged dinuclear Dy single-molecule magnet†

William R. Reed,[a] Maja A. Dunstan,[a] Robert W. Gable,[a] Wasinee Phonsri,[b] Keith S. Murray,[b] Richard A. Mole[c] and Colette Boskovic*[a]

Dedicated to Professor Annie Powell on the occasion of her 60th birthday.

Abstract

Two families of neutral tetraoxolene-bridged dinuclear rare earth complexes of general formula [((HBpz$_3$)$_2$RE)$_2$(μ-tetraoxolene)] (RE = Y and Dy; HBpz$_3^-$ = hydrotris(pyrazolyl)borate; tetraoxolene = fluoranilate (fa^{2-}; **1-RE**) or bromaniliate (ba^{2-}; **2-RE**)) have been synthesised and characterised. In each case, the bridging tetraoxolene ligand is in the diamagnetic dianionic form and each rare earth metal centre has two HBpz$_3^-$ ligands completing the coordination. Electrochemical studies on the soluble **2-RE** family reveals a tetraoxolene-based reversible one-electron reduction. Bulk chemical reduction with cobaltocene affords the cobaltocenium ($CoCp^+$) salt of the 1e-reduced analogue: [CoCp][((HBpz$_3$)$_2$RE)$_2$(μ-ba$^{\bullet}$)] (**3-RE**) that incorporates a radical trianionic form of the bromanilate bridging ligand. Alternating current (ac) magnetic susceptibility studies of **2-Dy** reveal slow magnetic relaxation only in the presence of an applied magnetic field, but reduction to radical-bridged **3-Dy** affords frequency-dependent peaks in the out-of-phase ac susceptibility in zero applied dc field. Exchange coupling between the Dy(III) ions and the radical bridging ligand thus reduces zero-field magnetisation quantum tunnelling and confers single-molecule magnet status on the complex.

Comprehensive analysis of the magnetic relaxation data indicates that a combination of Orbach, Raman and direct relaxation processes are required to fit the data for both dysprosium complexes.

Introduction

The last few years have seen the most significant advances in the field of single-molecule magnets (SMMs) since the discovery that lanthanoid complexes could exhibit the signature SMM properties of slow magnetic relaxation and magnetisation quantum tunnelling.[1–6] Very recently several groups have reported a variety of dysprosium bis(cyclopentadienyl) SMMs that exhibit magnetisation hysteresis around liquid nitrogen temperature.[7–10] These advances have taken SMMs well above liquid helium temperature, paving the way for real applications of SMMs based on bistability. Also illuminating, are recent advances in elucidating the role that different mechanisms play in SMM relaxation.[4,11–13] The importance of Raman processes, in addition to Orbach relaxation has become much more evident, as has the role of features beyond the molecule, including the involvement of molecular vibrations and optical phonons.[14–17]

Although desirable for some applications, including quantum computing, quantum tunnelling of the magnetisation (QTM) prevents many lanthanoid(III) complexes from exhibiting open hysteresis loops at zero field, particularly for Kramers ions such as Dy(III). One approach to inhibiting this zero-field QTM has been to incorporate exchange-coupling into the systems. The most notable examples are N_2^{3-} radical-bridged dinuclear lanthanoid(III) complexes, the Tb(III) analogues of which exhibit magnetisation hysteresis as high as 30 K.[18–20] Other radical-bridged lanthanoid(III) SMMs have also been reported.[21–23]

A class of bridging ligands that is appealing for accessibility in radical forms is tetraoxolene, or anilate ligands (Chart 1), as well as their imino analogues. As well as being excellent ligands for discrete complexes and coordination polymers of d-block metal ions,[24–28] they are eminently suitable for

coordination to oxophilic lanthanoid(III) ions. Crystal structures of the dinuclear chloranilate-bridged complexes [((HBpz$_3$)$_2$RE$_2$(ca)] (HBpz$_3^-$ = hydrotris(pyrazolyl)borate; RE = Eu, Tb, Yb; ca^{2-} = chloranilate) were reported in 2004 featuring the diamagnetic dianionic form of the ligand.[29] In 2017 SMM slow magnetic relaxation in the absence of an applied magnetic field was reported by some of us and others for [((HBpz$_3$)$_2$Dy$_2$(tetrox)] (tetrox = chloraniliate and doubly deprotonated 2,5-dihydroxy-3,6-dimethylbenzo-1,4-quinone, in the diamagnetic dianionic forms).[30,31] Very recently, field-induced SMM properties have also been observed for the Er(III) and Yb(III) chloranilate complexes.[32] Both of these reports on the Dy(III) chloranilate SMMs also describe unsuccessful efforts to access analogues with a one-electron reduced radical form of the tetraoxolene ligand by reducing the parent dinuclear complex with coboltacene in toluene. More recently, van Slageren et al. reported this reduction successful when tetrahydrofuran (THF) was used instead, affording analogues with the chloranilate ligand in the radical trianionic form.[33] The radical-bridged Dy complex indeed proved to have better SMM properties than the parent compound. In addition, the Gd(III)-radical coupling was determined for the spin-only Gd(III) analogue to be antiferromagnetic and of moderate magnitude (J = 3-4 cm^{-1}, $\mathcal{H}$ = -2$J\hat{S}_{rad}\cdot\hat{S}_{Gd}$) from magnetic susceptibility and high field EPR spectroscopy. Although the nature and magnitude of the Dy(III)-radical coupling cannot be directly inferred from that of the Gd(III) analogue, clearly the exchange-coupling enhanced the SMM properties of the Dy(III) complex by decreasing the zero-field QTM.

Chart 1

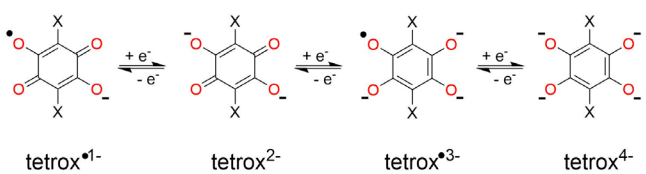

Our aim at the outset of the present work was to investigate the fluoranilate (fa^{2-}) analogue of

this family of dinuclear complexes, in anticipation that the more electronegative character of the fluorine substituents would increase the reduction potential and facilitate reduction and stability of the 1e-reduced radical-bridged analogue. We also opted to investigate the bromanilate (ba^{2-}) complexes for comparison. We report herein our exploration of the Y(III) and Dy(III) compounds [$((HBpz_3)_2RE)_2(\mu$-fa)] (**1-RE**) and [$((HBpz_3)_2RE)_2(\mu$-ba)]$\cdot 2CH_2Cl_2$ (**2-RE**) and the products of their chemical reduction.

Results and Discussion

Synthesis

The complexes **1-RE** and **2-RE** were synthesised following modification of the literature procedures employed for the chloranilate analogues.[29–31,33] Four equivalents of $KHBpz_3$ were added to a stirred solution containing two equivalents of rare-earth chloride salt. The faH_2 or baH_2 proligands were doubly deprotonated with Et_3N and added dropwise to an unstirred suspension of the rare-earth mixture with gentle swirling to dissolve the resulting suspension. A fine white precipitate was removed by filtration and the filtrate left to stand, affording crystalline samples of blue **1-RE** and purple **2-RE**, including crystals suitable for X-ray structure determination. While bromanilate compounds **2-Y** and **2-Dy** were analytically pure, the fluoranilate analogues were insoluble in all common organic solvents (e.g. tetrahydrofuran, simple alcohols, acetone, acetonitrile, chloroform, dichloromethane, ethyl acetate, hexane, DMF and DMSO) and their insolubility prevented purification by recrystallisation. In contrast, compounds **2-RE** are soluble in polar solvents.

As compounds **2-RE** are soluble, our efforts to access a radical-bridged analogue focused on these bromanilate-bridged complexes and employed the method developed by van Slageren *et al.*.[33] The reactions to afford compounds with the 1e-reduced complex, $[CoCp_2][((HBpz_3)_2RE)_2(\mu\text{-}ba^{\bullet})]$ (**3-RE**), were performed anaerobically using dry THF. Compounds **3-RE** were obtained as yellow-green

precipitates upon addition of a solution of one equivalent of cobaltocene to a purple solution of **2-RE**. The solid products are air-stable and analytically pure. Compounds **3-RE** are stable in anaerobic anhydrous MeCN, at least on the timescale of hours, but oxidise very rapidly upon exposure of the solution to air, affording a pink solution. The pink compound may be the bromanilate analogue $CoCp_2[RE(HBpz_3)_2(ba)]$ of the pink mononuclear complex reported previously, which arose from their attempt to reduce the parent dinuclear complex in toluene.[31] However, as van Slageren *et al*. reported for the reduced chloranilate analogue,[33] all attempts to recrystallise the compounds to access single crystals suitable for structure determination were unsuccessful.

Elemental analysis confirms the purity of the bulk samples of **2-Dy** and **3-Dy**, for which magnetochemical data are reported herein, as well as of **2-Y** and **3-Y**. The powder X-ray diffraction data (Fig. S1) measured for the bulk samples of **2-RE** (RE = Dy and Y) are in good agreement with diffractograms calculated from the single crystal structures, confirming the composition of the bulk samples. Thermogravimetric analysis (Fig. S2) of **2-RE** and **3-RE** is consistent with dichloromethane solvation and no solvation, respectively, as by elemental analysis. Integration of the ^{1}H NMR spectrum of diamagnetic **2-Y** further confirms the extent of dichloromethane solvation.

Structure descriptions

The single-crystal X-ray diffraction data for compounds **1-Dy**, **1-Y**, **2-Dy** and **2-Y** are presented in Table 1. Compounds **1-Dy**, **1-Y**, **2-Dy**, **2-Y** all crystallise in the monoclinic space group $P2_1/n$ with half a dinuclear complex per asymmetric unit. Compounds **1-RE** crystallise solvent-free as blue needles while compounds **2-RE** crystallise as purple plates with one dichloromethane molecule per asymmetric unit. Compounds **1-RE** are isomorphous with previously reported analogues with 2,5-dihydroxybenzoquinone, while compounds **2-RE** are isomorphous with previously reported chloranilate analogues with the same solvation.[29–31,33]

Table 1 Crystal data for compounds **1-Dy**, **1-Y**, **2-Dy** and **2-Y**.

	1-Dy	**1-Y**	**2-Dy**	**2-Y**
Empirical formula	$C_{42}H_{42}B_4Dy_2F_2N_{24}O_5$	$C_{42}H_{42}B_4F_2N_{24}O_5Y_2$	$C_{44}H_{44}B_4Br_2Cl_4Dy_2N_{24}O_4$	$C_{44}H_{44}B_4Br_2Cl_4N_{24}O_4Y_2$
Formula weight	1369.23	1222.05	1642.89	1495.71
Temperature/K	100(2)	100(2)	100.01(10)	100.01(10)
Crystal system	monoclinic	monoclinic	monoclinic	monoclinic
Space group	$P2_1/n$	$P2_1/n$	$P2_1/n$	$P2_1/n$
a/Å	11.790(2)	11.780(2)	14.1280(4)	14.0880(4)
b/Å	18.470(4)	18.470(4)	15.0635(4)	15.0798(3)
c/Å	12.250(3)	12.240(2)	14.8028(4)	14.8048(3)
α/°	90	90	90	90
β/°	104.23(3)	104.13(3)	108.024(3)	107.921(3)
γ/°	90	90	90	90
V/Å^3	2585.7(10)	2582.5(10)	2995.68(14)	2992.60(13)
Z	2	2	2	2
ρ_{calc}/g.cm^{-3}	1.759	1.572	1.821	1.660
μ/mm^{-1}	2.945	2.313	16.923	3.507
F(000)	1344.0	1236.0	1596.0	1488.0
Crystal size/mm^3	0.033 × 0.008 × 0.008	0.026 × 0.01 × 0.009	0.043 × 0.034 × 0.019	0.278 × 0.101 × 0.044
Radiation	Synchrotron (λ = 0.710900)	Synchrotron (λ = 0.710900)	Cu Kα (λ = 1.54184)	Mo Kα (λ = 0.71073)
2Θ range/°	4.078 to 56.564	4.08 to 56.56	7.562 to 148.926	4.796 to 56.564
Index ranges	$-15 \le h \le 15$, $-24 \le k \le 24$, $-15 \le l \le 16$	$-15 \le h \le 15$, $-24 \le k \le 24$, $-16 \le l \le 16$	$-15 \le h \le 17$, $-18 \le k \le 18$, $-18 \le l \le 16$	$-17 \le h \le 14$, $-16 \le k \le 19$, $-18 \le l \le 19$
Reflections collected	84712	84085	21304	23599
Independent reflections	6424 [R_{int} = 0.0680, R_{sigma} = 0.0259]	6410 [R_{int} = 0.0885, R_{sigma} = 0.0337]	6046 [R_{int} = 0.0428, R_{sigma} = 0.0411]	7000 [R_{int} = 0.0272, R_{sigma} = 0.0290]
Data/restraints/ parameters	6424/0/353	6410/0/353	6046/0/380	7000/0/379
Goodness-of-fit on F^2	1.040	1.011	1.100	1.058
Final R indexes [$I \ge 2\sigma(I)$]	R_1 = 0.0331, wR_2 = 0.0803	R_1 = 0.0451, wR_2 = 0.1135	R_1 = 0.0314, wR_2 = 0.0751	R_1 = 0.0282, wR_2 = 0.0685
Final R indexes [all data]	R_1 = 0.0456, wR_2 = 0.0855	R_1 = 0.0654, wR_2 = 0.1263	R_1 = 0.0351, wR_2 = 0.0766	R_1 = 0.0352, wR_2 = 0.0708
Largest diff. peak/ hole / e Å^{-3}	0.86/-1.48	0.58/-0.93	0.65/-0.74	0.59/-0.58

The neutral dinuclear rare-earth complexes in **1-Dy**, **1-Y**, **2-Dy** and **2-Y** are isostructural (Fig. 1), allowing for the different substituents on the bridging tetraoxolene ligands. The rare-earth centres are all eight coordinate with a $\{N_6O_2\}$ coordination sphere arising from coordination to two tripodal $HBpz_3^-$ ligands and the bis-bidentate tetraoxolene bridging ligand. The coordination geometries are closest to either square antiprismatic (**1-RE**) or triangular dodecahedral (**2-RE**) according to continuous shape analysis (Table 2) performed with the Shape 2.1 software.[34–36] The previously reported chloranilate analogues have been found to exhibit both square antiprismatic and triangular dodecahedral coordination, depending on solvation.[30,31,33] Bond length analysis of the yttrium analogues shows similar Y-O and Y-N bond lengths for all complexes, in the respective ranges 2.3–2.4 and 2.4–2.6 Å. As is typical for Dy and Y analogues, the Dy-O/N bond in **1-Dy** and **2-Dy** are slightly longer than the equivalent Y-O/N bonds in **1-Y**. Tetraoxolene C-C and C-O bond lengths are all consistent with the dianionic oxidation state assigned, with the ligand adopting a delocalised bis-bidentate binding mode.[24] The shortest intermolecular RE···RE distances of 8.0–8.8 Å are shorter in some cases than the intramolecular distances of 8.5–8.7 Å.

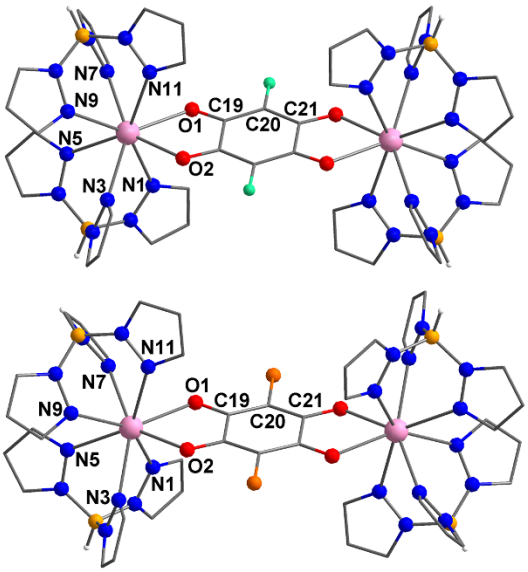

Fig. 1 Structural representations of the dinuclear complexes in **1-RE** (top) and **2-RE** (bottom). Pyrazole hydrogen atoms have been omitted for clarity. Colour code: Y (pink), O (red), N (blue), B (orange), F (green), Br (brown), C (black), H (white).

Table 2 Selected interatomic distances (Å) and SHAPE parameters for **1-Dy**, **1-Y**, **2-Dy** and **2-Y**.

Parameter	**1-Dy**	**1-Y**	**2-Dy**	**2-Y**
Distance				
RE-O[a]	2.347(3), 2.384(3)	2.338(2), 2.368(2)	2.359(3), 2.369(3)	2.357(2), 2.358(2)
RE-N	2.434(4) – 2.562(3)	2.424(3) – 2.547(3)	2.428(3) – 2.549(3)	2.420(2) – 2.544(2)
C-O[a]	1.259(5), 1.261(5)	1.254(4), 1.259(3)	1.256(4), 1.257(5)	1.252(3), 1.258(3)
C_{19}-C_{21} (C_{10}-C_{11}, C_{13}-C_{14})[b]	1.533(5)	1.536(3)	1.542(4)	1.540(3)
C_{19}-C_{20}, C_{20}-C_{21} (C_{10}-C_{15}, C_{12}-C_{13})[a]	1.389(5), 1.391(5)	1.390(4), 1.395(4)	1.390(5), 1.390 (5)	2.392(3), 1.400(3)
Intramolecular RE···RE	8.623(2)	8.600(1)	8.6434(5)	8.6265(5)
Intermolecular RE···RE[b]	8.059(3)	8.065(2)	8.7050(5)	8.7038(4)
Shape Parameters[c]				
DD-8	1.32	1.34	0.788	0.756
SAPR-8	0.723	0.699	2.27	2.29

[a]Tetraoxolene. b[c]Shortest distance. [c]Shape abbreviations: DD-8: triangular dodecahedron, SAPR-8: square antiprism.

Compounds **1-RE** crystallise solvent-free and exhibit intermolecular π-π stacking (3.3 Å) of the pyrazole rings (Fig. S3). This affords relatively short intermolecular RE···RE distances and likely accounts for the relative insolubility of these compounds. Analogous intermolecular interactions are not evident for compounds **2-RE**, which exhibit similar crystal packing (Fig. S4) to the previously reported chloranilate analogues.

Infrared, electronic and EPR spectroscopy

The infrared spectra of **2-RE** and **3-RE** were measured as pressed KBr disks (Fig. S5). The spectra of the Y versus Dy analogues of the **2-RE** and **3-RE** families show minimal variation, consistent with the isostructural nature of the complexes. All spectra exhibit strong vibrational modes attributed mostly to stretches associated with the $HBpz_3^-$ ligand. A single B-H stretch of the $HBpz_3^-$ is seen at ~ 2450 cm^{-1}, confirming the presence of the coordinated tripodal ligand. The C-O stretch of the bridging ligand fluoranilate appears at ~1545 cm^{-1}, while the C-O stretch for bromanilate shifts to ~1530 cm^{-1} due to the less electronegative bromo substituents. The spectra of **3-RE** exhibit an intense band at 1456 cm^{-1} which is assigned to the C-O$^{\cdot}$ radical stretch of the trianionic radical bromanilate ligand.[27] The cobaltocenium cation also affords vibrational modes for **3-RE** at 1013 cm^{-1}, 858 cm^{-1} and 501 cm^{-1} from an sp^2 C-H in-plane bend, an sp^2 C-H out-of-plane bend, and a cyclopentadienyl tilt respectively.[37]

Electronic UV-visible spectra were measured in diffuse reflectance mode for solid samples diluted in KBr and in absorbance mode for MeCN solutions of compounds **2-Dy** and **3-Dy** (Fig. 2). Diffuse reflectance spectra were also measured for fluoranilic and bromanilic acid (Fig. S6). The intense band at ~350 nm evident for all complexes is assigned as a ligand centered π - π^* transition and the broad band over the visible range is assigned as a n - π^* transition.[38] Upon the reduction of **2-Dy** to **3-Dy**, the band in the visible is slightly blue-shifted, due to the destabilisation of the π^* orbital. Several additional bands are evident for **3-Dy** and the spectra resemble the solution absorption spectrum for the analogous

chloranilate compound, monitored spectroscopically during electrochemical reduction.[33] The additional features include a band at 266 nm which is assigned to the cobaltocenium cation.[39] In addition[31], the fine structure in the range 400-500 nm, has been assigned to a π - π^* transition centred on the radical trianionic bromaniliate ligand, with vibronic coupling to the delocalised radical.[33,38] After exposure of the anaerobic solution of **3-Dy** to the atmosphere, the solution rapidly changes from yellow-green to pink (Fig. S7), due to decomposition, possibly to the previously discussed mononuclear complex.

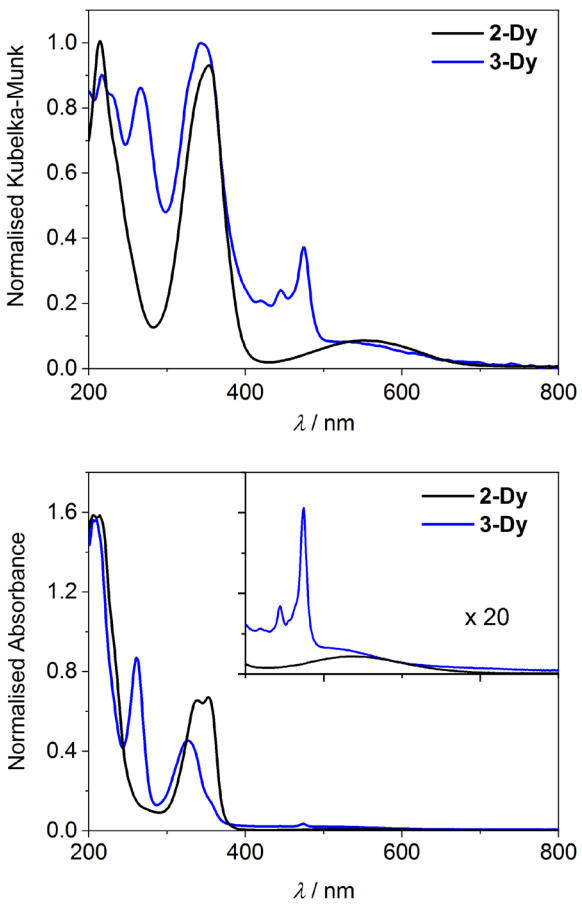

Fig. 2 UV-visible spectra measured for **2-Dy** (black) and **3-Dy** (blue) as diffuse reflectance dispersed in KBr (above) and as absorbance in MeCN solution (below).

The room temperature X-band EPR spectrum of a powder sample of **3-Y** exhibits a featureless isotropic band centred at g = 1.995 (Fig. S8). This is consistent with the S = 1/2 radical trianionic form of the bromanilate ligand.[40]

Electrochemistry

Following confirmation of solution stability of **2-Y** by ^{1}H NMR spectroscopy, the voltammetric behaviour of solutions of **2-Y** and **2-Dy** were examined by cyclic (CV) and rotating disk electrode (RDE) voltammetry. Voltammograms were measured in dry acetonitrile with an analyte concentration of 0.5 mM and 0.25 M $(Bu_4N)(PF_6)$ as the supporting electrolyte with a glassy carbon working electrode (Figs. 3 and S9). For quasi-reversible processes, the mid-point potentials (E_m) and peak-to-peak separations (ΔE_p) from CV data are tabulated in Table 3, together with the half-wave potentials ($E_{1/2}$) and limiting currents (i_L) from RDE voltammetry. For the irreversible oxidations, the oxidation peak potentials (E_{pa}) obtained by cyclic voltammetry with 100 mVs^{-1} scan rate are also tabulated. All potentials are quoted versus the ferrocene/ferrocenium (Fc/Fc^+) couple.

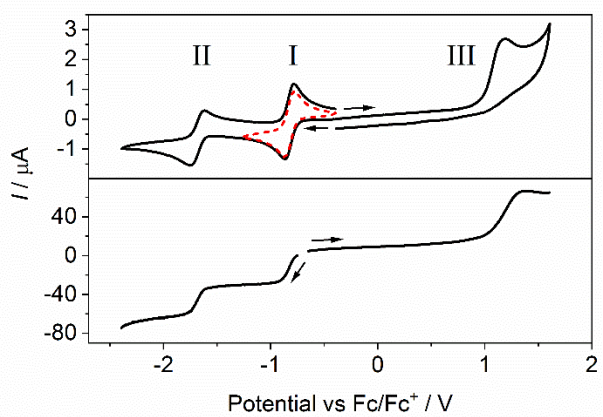

Fig. 3 Cyclic and RDE voltammograms of **2-Dy** (0.5 mM in MeCN with 0.25 M Bu_4NPF_6) obtained with a 3 mm diameter glassy carbon working electrode at a scan rate of 100 or 20 mVs^{-1}, for CV and RDe, respectively. The dashed red lines plot the voltammograms measured with a switching potential

immediately past the first reduction to probe reversibility. The anodic and cathodic regions were scanned separately as indicated by the arrows.

Table 3 Table of electrochemical parameters for **2-Dy**, **2-Y** and **3-Dy**.

	Reductions				**Oxidation**	
Compound	**I**		**II**		**III**[b]	
	E_m / V (ΔE_p / mV)	$E_{1/2}$ / V (i_L / μA)	E_m / V (ΔE_p / mV)	$E_{1/2}$ /V (i_L / μA)	E_{pa}[a] / V	$E_{1/2}$ / V (i_L / μA)
2-Dy	–0.82 (90)	–0.82 (33)	–1.68 (140)	–1.69 (29)	1.19	1.16 (51)
2-Y	–0.83 (80)	–0.82 (29)	–1.69 (160)	–1.78 (19)	1.35	1.21 (41)
3-Dy	–0.82 (80)	-	–1.68 (75)	-	1.23	-

[a] E_{pa} at a scan rate of 100 mVs^{-1}
[b] E_m and i_L cannot be determined for an irreversible process

The complexes **2-Y** and **2-Dy** each exhibit three redox processes at similar potentials within the measured potential window. The position of zero current in the RDE voltammograms confirm these as two reductions (processes I and II) and an oxidation (process III) (Table 3, Figs. 3 and S9). The three processes are all assigned as bromanilate-based processes (Scheme 1), consistent with literature analogues with other tetraoxolene ligands.[30,33] Processes I-III shift depending on the tetraoxolene substituent.[30] For **2-Dy**, the E_m values of both reductions are independent of scan rate at –0.82 V and –1.68 V for processes I and II, respectively. The current ratios i_{pa}/i_{pc} for process I are close to unity, where i_{pa} and i_{pc} are the peak anodic and peak cathodic currents respectively. Process I has a ΔE_p of 90 mV at a scan rate of 100 mVs^{-1}, which is as reversible as the Fc/Fc^+ couple under these conditions, consistent with the assignment of I as a diffusion controlled and reversible one-electron process. Process II has a ΔE_p of 140 mV and the current ratio i_{pa}/i_{pc} is less than one, consistent with assignment of process II as quasi-reversible. The oxidation process III shows no current response on the reverse sweep and is clearly irreversible. The RDE limiting currents are comparable for processes I and II, consistent with both

processes involving the transfer of one electron, while the limiting current cannot be determined for the irreversible oxidation, process III. The voltammetry for **2-Y** is very similar to that for **2-Dy** (Fig. S9), consistent with the observed processes all being ligand-based. The voltammograms and redox potentials for **2-Y** and **2-Dy** are comparable to those for the chloranilate analogues in the same conditions.[30]

Scheme 1 Electrochemical processes (I, II and III) for **2-RE** and analogues

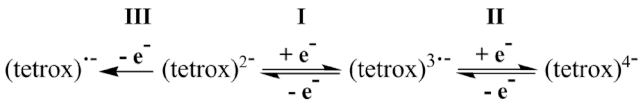

Cyclic voltammograms were also obtained for one-electron reduced analogue **3-Dy** under rigorously dry and degassed conditions (Fig. S10, Table 3). The three processes observed for **2-Dy** are also evident in the voltammogram of **3-Dy**, with the same potentials and similar ΔE_p for the reversible processes. For compound **3-Dy**, process I is now assigned as a 1e-oxidation of the trianionic radical form of the bromanilate bridging ligand to the dianionic form (Scheme 1). There is also a reversible reduction of cobaltocenium to cobaltocene at -1.34 V (ΔE_p = 90 mV).[41] On the anodic scan, two additional low intensity processes at 0.40 and 0.72 V are evident. Upon exposure to air, the solution becomes pink and these processes increase in intensity, while processes I, II and III disappear, indicating that these additional processes are associated with the decomposition product/s.

Static magnetic properties

Magnetic susceptibility data were acquired for analytically pure bulk samples of **1-Dy** and **3-Dy**. Variable temperature magnetic susceptibility measurements (Fig. 4) were measured between 2 and 300 K with an applied field of 1000 Oe. The room temperature $\chi_M T$ value for **2-Dy** is 28.2 $cm^3\ mol^{-1}\ K$, which is in good agreement with the expected value of 28.4 $cm^3\ mol^{-1}\ K$ for two non-interacting Dy(III) ions ($^6H_{15/2}$: 28.3 $cm^3\ mol^{-1}\ K$). Upon incorporation of a S = 1/2 (g = 2.0) radical ligand, the room

temperature $\chi_M T$ value expected for **3-Dy** is 28.8 $cm^3 mol^{-1} K$ and the measured value of 27.5 $cm^3\ mol^{-1}$ K is within 5% of this value. Upon decreasing temperature, $\chi_M T$ gradually decreases for **2-Dy** to reach a value of 24.0 $cm^3\ mol^{-1}$ K at 3.4 K, before decreasing more rapidly to a value of 23.1 $cm^3\ mol^{-1}$ K at 2.45 K. The thermal profile is similar to that measured previously for the chloranilate analogue.[30,33] The gradual decrease at higher temperatures is attributed to the progressive depopulation, upon decreasing temperature, of the excited levels arising from the crystal field splitting of the ground *J* multiplets of Dy(III). Upon decreasing temperature $\chi_M T$ also gradually decreases for **3-Dy**, reaching a broad local minimum value of 25.7 $cm^3\ mol^{-1}$ K at 55 K before then increasing to a value of 31.4 $cm^3\ mol^{-1}$ K at 7.5 K and finally decreasing to 27.7 $cm^3\ mol^{-1}$ K at 1.9 K. Qualitatively, this profile strongly resembles that of the analogous complex with the radical trianionic chloranilate bridging ligand. The low temperature maximum in $\chi_M T$ has been ascribed to the effect of coupling between the Dy(III) centres and the radical ligand. The orbital angular momentum of Dy(III) prevents ready determination of the exchange coupling from the magnetic susceptibility data;[42] however, magnetic susceptibility and high field EPR studies on the spin-only Gd(III) analogue of the chloranilate complex suggest antiferromagnetic coupling of moderate strength.[33]

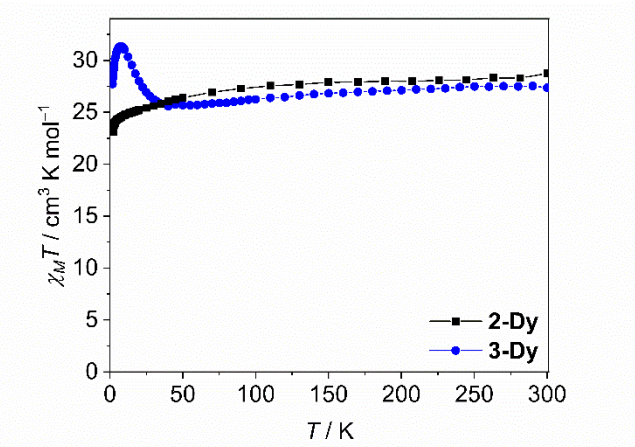

Fig. 4 Plot of $\chi_M T$ versus T for **2-Dy** and **3-Dy**. The lines are a guide for the eye.

Magnetisation versus field data (Figs. S11 and S12) were measured for **2-Dy** and **3-Dy** between 1.8 and 7 K with fields up to 5 T. For both compounds the M vs H isotherms saturate at the lowest temperatures near 10 μ_B, which is consistent with isolated ground states comprised mainly of $^6H_{15/2}$ microstates with the maximum $m_J = \pm 15/2$. The observed saturation value for **3-Dy** is lower than that for **2-Dy**, consistent with antiferromagnetic coupling between the two Ln(III) centres and the radical ligand.

Dynamic magnetic properties

Alternating current (ac) magnetic susceptibility data were measured for **2-Dy** and **3-Dy** in the temperature range 2–25 K and frequency (ν) range 10-10,000 Hz to probe the effect of exchange-coupling on the SMM behaviour (Figs. 5 and S13-S14). At a temperature of 2.5 K and zero applied dc field (B_{dc}), compound **2-Dy** does not exhibit an appreciable out-of-phase (χ_M'') signal until the ac frequency is over 1,000 Hz (Fig. S13), suggesting rapid QTM. Variable field measurements at 2.5 K identified the lowest dc field to afford a clearly defined maximum in χ_M'' as 375 Oe. Variable frequency, variable temperature measurements at an applied field of 390 Oe show temperature-dependent maxima at lower frequencies, as well as the tail of a second process at frequencies higher than the range of the instrument. consistent with a dominant QTM process. Above 2.9 K, there is a thermal dependence and peak maxima are evident at temperatures up to 10 K below the highest accessible ac frequency of 10,000 Hz. In contrast, the radical-bridged **3-Dy** exhibits frequency-dependent χ_M'' peak maxima in zero applied dc field, again with some temperature-invariance at the lowest temperatures, indicative of QTM. A field scan at 2.5 K shows a field-dependence of χ_M'' and a field of 380 Oe was chosen for comparison with the measurements on **2-Dy** (Fig. S14). Measurement of variable temperature, variable frequency ac susceptibility data with this applied field affords peaks in accessible frequency range for temperatures

up to 5 K.

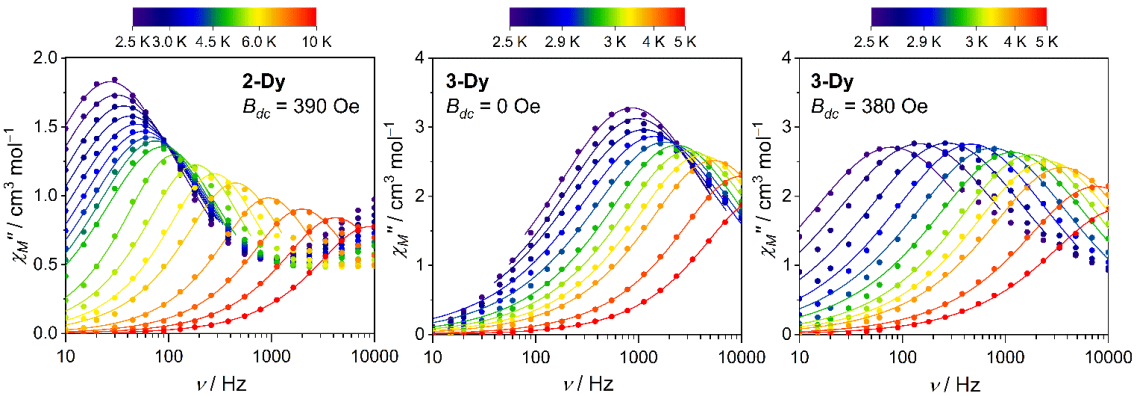

Fig. 5 Frequency-dependence of the out-of-phase ac magnetic susceptibility (χ_M'') in the temperature range 2.5–10 K for **2-Dy** with B_{dc} = 390 Oe (left), and in the temperature range 2.5 – 5 K for **3-Dy** with zero applied field (centre) and **3-Dy** with B_{dc} = 380 Oe (right). The lines are best fits to the Debye equation as described in the text.

The χ_M'' isotherms measured for **2-Dy** and **3-Dy** from the variable temperature and frequency ac susceptibility measurements were fit, where possible, to the Debye equation to obtain the characteristic relaxation time (τ) and lifetime distribution (α) at each temperature (Table S1). For **2-Dy**, only the low frequency process was fit up to 10 K, while for **3-Dy** the isotherms could only be reliably fit up to 5 K. The values of the α parameters from these fits indicates a range of lifetimes in all cases. To investigate the mechanisms responsible for the slow relaxation observed for **2-Dy** and **3-Dy**, the $\tau(T)$ data were fit to the relaxation expression:

$$\tau^{-1} = \tau_0^{-1} \exp\left(-U_{eff}/k_B T\right) + CT^n + AT + {\tau_{QTM}}^{-1} \qquad \textbf{(1)}$$

where τ_0 is the pre-exponential factor and U_{eff} the effective energy barrier of an Orbach process, C and n are the Raman constants, A is the direct relaxation coefficient, and τ_{QTM} is the QTM relaxation time. Initial efforts to fit the data solely to an Orbach process (Fig. S15, Table S2) afforded U_{eff} and τ_0 values of 52 ± 4 K and (6.8 ± 3.3) × 10^{-7} s, 20.8 ± 0.4 K and (1.6 ± 0.1) × 10^{-7} s, and 25.8 ± 0.3 K and (7.4 ± 0.5) × 10^{-8} s for **2-Dy** with B_{dc} = 390 Oe, **3-Dy** with B_{dc} = 0 and **3-Dy** with B_{dc} = 380 Oe, respectively. While a satisfactory fit is obtained for **3-Dy** in an applied field, the fit at lower temperature is poor in the other two cases and the three pre-exponential factors are rather high. To explore the possibility of Raman relaxation, the data were plotted as log-log plots (Fig S15) and fit to only the Raman term in eq. 1.[43] In each case a satisfactory fit of the lower temperature data was not obtained while fitting the higher temperature data afforded the n (C) parameters of 5.8 ± 0.2 and 0.084 ± 0.044 s K^{-n}, 4.8 ± 0.1 and 42 ± 8 s K^{-n}, and 6.7 ± 0.2 and 1.8 ± 0.6 s K^{-n} for **2-Dy** with B_{dc} = 390 Oe, **3-Dy** with B_{dc} = 0 and **3-Dy** with B_{dc} = 380 Oe, respectively (Table S2).

After the initial fit attempts assuming only an Orbach or Raman process were found inadequate to fit all data, the data for **2-Dy** were fit to Eq. 1 assuming a combination of non-zero direct, Orbach and Raman processes, while the inclusion of a QTM term gave no reasonable values of τ_{QTM}. This is consistent with having chosen the applied field at which QTM is negligable. The Raman exponent, n, gave similarly good fits for values of 5 and 7, with a similar direct relaxation coefficient, but different Orbach relaxation terms. The best fit with n = 7, expected for Dy(III), gave A = 52 ± 8 s^{-1} K^{-1}, C = (5.21 ± 0.06) × 10^{-3} s K^{-7}, U_{eff} = 7 ± 1 K and τ_0 = (1.4 ± 0.2) × 10^{-4} s (Fig. 6, Table 3).[44]

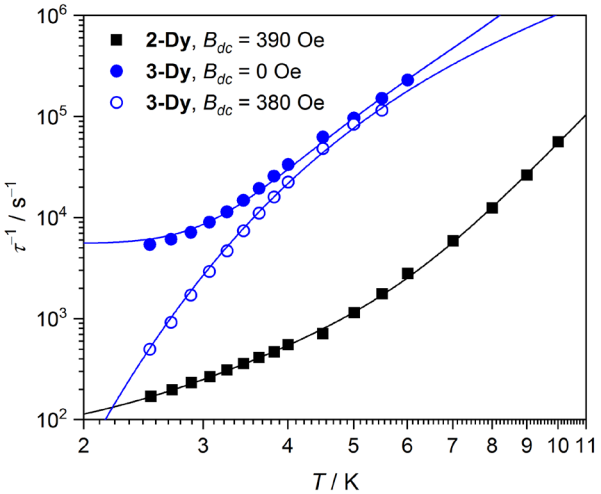

Fig. 6 Relaxation time plots for **2-Dy** (B_{dc} = 390 Oe, black) and **3-Dy** (B_{dc} = 0 Oe, blue closed circles; B_{dc} = 380 Oe, blue open circles).

Table 3 Parameters of best fit obtained from fitting the ac relaxation data for **2-Dy** and **3-Dy** to eq. 1 as described in the text.

	2-Dy	**3-Dy**	**3-Dy**
B_{dc} / Oe	390	0	380
τ_0 / s	$(1.4 \pm 0.2) \times 10^{-4}$	$(9.6 \pm 0.1) \times 10^{-8}$	$(8.6 \pm 0.9) \times 10^{-8}$
U_{eff} / K	7 ± 1.1	10.4 ± 0.1	10.6 ± 0.2
C / s K^{-n}	$(5.21 \pm 0.06) \times 10^{-3}$	0.150 ± 0.01	9.00×10^{-3} (fixed)
n	7 (fixed)	7 (fixed)	7 (fixed)
A / s^{-1} K^{-1}	52 ± 8	0 (fixed)	2.15×10^{-2} (fixed)
τ_{QTM} / s	-	$(1.8 \pm 0.1) \times 10^{-4}$	0 (fixed)

Analogous efforts to fit the $\tau(T)$ data for **3-Dy** in applied fields of 0 and 380 Oe to Eq. 1 afforded multiple satisfactory, including various combinations of relaxation processes. In an effort to narrow down the sets of possible fit paramaters, we explored fitting the relaxation time data taking into account the field-dependence of the Raman, Direct and QTM parameters (ESI-Discussion S1, Eq. S1). [45–47] The isofield lines obtained at 2.5 K were fit with the Debye equation (Table S3). The full set of $\tau(T,B)$ data were then fit simultaneously to give field-dependent relaxation parameters (Fig. S16, Table S4), which were used as initial values in fitting the $\tau(T)$ data at 0.085 and 380 Oe to Eq. 1. For the zero-field data, the calculated direct relaxation coefficient, A, was exceedingly small and thus fixed to 0, while the best fit gave values $\tau_{QTM} = (1.8 \pm 0.1) \times 10^{-4}$ s, $C = 0.150 \pm 0.01$ s K^{-7}, $U_{eff} = 10.4 \pm 0.1$ K, $\tau_0 = (9.6 \pm 0.1) \times 10^{-8}$ s (Table 3, Fig. 6). In an applied field of 380 Oe, τ_{QTM} becomes so large that it does not contribute significantly to the magnetic relaxation, and was fixed to 0. The best fit obtained upon refinement with A and C fixed to 2.15×10^{-2} s^{-1} K^{-1} and $C = 9.00 \times 10^{-3}$ s K^{-7} gave $U_{eff} = 10.6 \pm 0.2$ K and $\tau_0 = (8.6 \pm 0.9) \times 10^{-8}$ s (Table 3, Fig. 6). In the absence of spectroscopic measurements or *ab initio* calculations to provide an indication of the electronic stucture in terms of the energies and m_J compositions of the low energy microstates, it is difficult to comment on the accuracy of the relaxation parameters obtained from the relaxation fits and the implications for the dominant relaxation process. Nevertheless, Orbach U_{eff} and τ_0 values and Raman n values are generally comparable to those obtained for the chloranilate analogues.[30,31,33]

Concluding remarks

The incorporation of two new tetraoxolene ligands has afforded two new families of dinuclear [((HBpz$_3$)$_2$RE)$_2$(μ-tetraoxolene)] complexes with fluoranilate and bromanilate bridging ligands. In principle, the fluoranilate analogue would be expected to be more readily reduced and to allow access to more stable 1e-reduced radical-bridged complexes. Unfortunately, strong supramolecular interactions

afford insoluble complexes that are not amenable to reduction.

Bromanilate proved more accommodating than fluoranilate and we were able to synthesise the target 1e-reduced radical-bridged dinuclear Dy(III) complex from the bromanilate analogue in the form of an air-stable solid. This complex exhibits SMM slow magnetic relaxation in zero applied dc magnetic field, in contrast to the parent complex with the diamagnetic bridge. As is the case for the chloranilate analogue, exchange coupling between the Dy(III) ions and radical ligand reduces the QTM at zero-field, enhancing the SMM properties. A combination of Orbach, Raman and direct relaxation processes are required to fit the magnetic relaxation data for both dysprosium complexes. Elucidation of the nature of the exchange coupling between the radical ligand and Dy(III) ions has not been possible in the present work and in general remains a considerable challenge that will likely only be surmounted when improved *ab initio* computational methodologies become available. Ultimately, determination of such exchange coupling is essential to understand the origin of the different magnetic relaxation pathways in exchange-coupled SMMs.

Experimental section

Materials and Methods

Compounds **1-RE** and **2-RE** were synthesised under aerobic conditions unless specified, while the synthesis and manipulation of compound **3-RE** was performed using using standard Schlenk techniques under an atmosphere of dry nitrogen. All chemicals purchased were of reagent grade or higher and used as received, except for the THF employed in the synthesis of **3-RE**, which was purified and dried using a MBRAUN solvent purification system and the MeCN employed for electrochemistry and solution UV-visible measurements, which was dried over activated molecular sieves (3 Å) for three days.[48] The $KHBpz_3$ proligand was prepared according to the literature procedure.[49]

Bromanilic acid (baH_2). A modified literature procedure was followed.[50,51] Liquid bromine (12.0 mL, 233 mmol) was slowly added to 2,5-dihydroxy-1,4-benzoquinone (6.32 g, 45.4 mmol) in acetic acid (100 mL). The deep red solution was heated slowly to 110°C with stirring for 18 hours. After cooling, a red crystalline precipitate was isolated by filtration, washed with cold acetic acid and air-dried (10 g, 75%). UV-visible (reflectance, in □5% KBr): λ_{max} 235, 326, 474 nm. FT-IR (KBr disc, cm^{-1}): ν_{CO} 1645 (s) 1609 (s), 1533 (s), 1380 (s), 1317 (m).

Fluoranilic acid (faH_2). A modified literature procedure was followed.[52] A yellow solution of fluoranil (1.37 g, 7.62 mmol) was dissolved in 1,4-dioxane (15 mL). An aqueous solution of NaOH (5.65 M, 40 mL) was added slowly while stirring. The resulting dark brown solution was stirred for 2 h at room temperature. The solution was acidified with HCl (32 %, 20 mL) to afford an orange precipitate that was isolated by filtration and air-dried. The crude product was dissolved in acetone to yield a red solution with some fine white precipitate, which was removed by filtration. The solvent was evaporated to dryness to afford a crystalline orange-brown precipitate, which was recrystallised from hot acetic acid to yield bright orange plates, which were isolated by filtration, washed with cold acetic acid and air-dried (0.80 g, 59 %). UV-visible (reflectance, in □5% KBr): λ_{max} 299, 460 nm. FT-IR (KBr disc, cm^{-1}): ν_{CO} 3475 (s) 1630 (s) 1294 (s) 997 (s).

[($(HBpz_3)_2Dy)_2$(μ-fa)] (1-Dy). Solid $DyCl_3 \cdot 6H_2O$ (100 mg, 0.330 mmol) was dissolved in EtOH (2.0 mL), then CH_2Cl_2 (10 mL) was added. Solid $KHB(pz)_3$ (166 mg, 0.660 mmol) was added to the reaction mixture to afford a colourless suspension that was stirred for 5 minutes. A deep blue solution of fa^{2-} was prepared by the addition of Et_3N (46 μL, 0.330 mmol) to faH_2 (29.1 mg, 0.165 mmol) in CH_2Cl_2 (5.0 mL). The deprotonated ligand was added dropwise to the colourless suspension, resulting in a deep blue solution with some fine precipitate, which was removed by filtration. The resultant filtrate was sealed and left to form a light blue microcrystalline product. Recrystallisation from EtOH/CH_2Cl_2

afforded crystals that were manually separated for structural analysis. It was not possible to obtain an analytically pure bulk sample.

[((HBpz$_3$)$_2$Y)$_2$(μ-fa)] (**1-Y**). The synthesis of the Y analogue followed that of the Dy-analogue, employing YCl_3 in place of $DyCl_3$.

[((HBpz$_3$)$_2$Dy)$_2$(μ-ba)]·2CH_2Cl_2 (**2-Dy**). Solid $DyCl_3·6H_2O$ (87.6 mg, 0.233 mmol) was dissolved in EtOH (5 mL), followed by addition of CH_2Cl_2 (5 mL). Solid $KHB(pz)_3$ (97.1 mg, 0.385 mmol) was added to the reaction mixture to afford a colourless suspension that was stirred for 5 minutes. A violet solution of ba^{2-} was prepared by the addition of Et_3N (24 μL, 0.172 mmol) to baH_2 (25.6 mg, 0.086 mmol) in EtOH/CH_2Cl_2 (4 mL). The ba^{2-} solution was added dropwise to the unstirred colourless Dy-containing suspension, resulting in a deep purple solution and some fine precipitate which was removed by filtration. The resultant filtrate was sealed and left to stand, affording purple parallelogram plate-shaped crystals (60 mg, 47 %). Single crystals suitable for X-ray diffraction were maintained in contact with mother liquor to prevent desolvation. UV-visible (reflectance, in □5% KBr): λ_{max} 215, 350, 560 nm. UV-visible (absorbance at 5×10^{-5} M in MeCN): λ_{max} 210, 337, 353, 541 nm. FT-IR (KBr disc, cm^{-1}): ν_{BH} 2466 (w), ν_{CO} 1538 (s), 1404 (s), 1300 (s), 1215 (s) 1050 (s). Anal. Calcd for $Dy_2C_{44}H_{44}N_{24}O_4B_4Cl_4Br_2$: C, 32.17; H, 2.70; N, 20.46. Found: C, 32.47; H, 2.62; N, 20.93.

[((HBpz$_3$)$_2$Y)$_2$(μ-ba)]·2CH_2Cl_2 (**2-Y**). Synthesis of the Y analogue followed that of the Dy-analogue, employing YCl_3 in place of $DyCl_3$; yield: 54 %. ^{1}H NMR (400 MHz, CD_3CN): δ = 6.09 (t, 12H), 6.97 (d, 12H), 7.79 (d, 12H). Anal. Calcd for $Y_2C_{44}H_{44}N_{24}O_4B_4Cl_4Br_2$: C, 35.58; H, 2.97; N, 22.73. Found: C, 35.59; H, 2.85; N, 22.91.

[CoCp][((HBpz$_3$)$_2$Dy)$_2$(μ-ba$^{\bullet}$)] (**3-Dy**). The complex **2-Dy** (140 mg, 0.095 mmol) was dissolved in THF (30 mL) affording a clear deep purple solution. Cobaltocene (19 mg, 0.100 mmol) was dissolved in THF (20 mL) and added to **2-Dy**, affording a yellow-green precipitate immediately. The suspension was stirred for 2 hours before the precipitate was isolated by filtration, washed with cold, THF (3 × 10

mL) and air-dried, yielding a yellow-green amorphous powder (95 mg, 60%). UV-visible (reflectance, in □5% KBr): λ_{max} 217, 229, 269, 350, 445, 474, 541 nm. UV-visible (absorbance at approximately 5×10^{-5} M in MeCN): λ_{max} 210, 260, 326, 444, 474, 532 nm. FT-IR (KBr disc cm^{-1}): ν_{BH} 2462 (m), ν_{CO} 1535 (s), 1404 (s), 1298 (s), 1215 (s), 1049 (s), $\nu_{CO\cdot}$ 1454 (s), $\nu CoCp_2^+$ 1011 (w), 860 (w). Anal. Calcd for $Dy_2CoC_{52}H_{50}N_{24}O_4B_4Br_2$: C, 37.58; H, 3.03; N, 20.22. Found: C, 37.85; H, 3.04; N, 20.13.

[CoCp][((HBpz$_3$)$_2$Y)$_2$(μ-ba$^{\cdot}$)] (**3-Y**). Synthesis of the Y-analogue followed that of the Dy-analogue; yield 57%. Anal. Calcd for $Y_2CoC_{52}H_{50}N_{24}O_4B_4Br_2$: C, 41.23; H, 3.33; N, 22.19. Found: C, 41.23; H, 3.25; N, 21.78.

X-ray Diffraction and Structure Solution

Crystals were transferred directly from the reaction mixture to oil. The crystallographic data (Table 1) for **2-Y** and **2-Dy** were collected, at 100 K, using a Rigaku Synergy Dual Wavelength Single Crystal X-ray Diffactometer with Cu-Kα (λ = 1.54018 Å) and Mo Cu-Kα (λ = 0.71073 Å) radiation, respectively. The data were reduced using CrysAlisPro[53] using a numerical absorption correction based on Gaussian integration over a multifaceted crystal model. Data for the remaining crystals were collected, at 100K, on the MX1 or MX2 beamlines at the Australia Synchrotron fitted with a silicon double crystal monochromator, the wavelength being tuned to approximately Mo-Kα radiation (λ = 0.7109 Å).[54,55] Data reduction was performed using XDS, using strong multi-scan absorption correction in SADABS.[56,57]

Using OLEX2[58] the structures were solved with the SHELXT structure solution program using Intrinsic Phasing and refined with the ShelXL refinement package using Least Squares minimisation on F^2, using all data.[59,60] All non-hydrogen atoms were refined with anisotropic displacement parameters, while all hydrogen atoms were placed at geometrical estimates and refined using the riding model. Both **1-RE** and **2-RE** structures had solvent voids, the latter two structures showed diffuse solvent equivalent to 0.5 molecules of water per formula unit and so refinement was carried out using the OLEX2 solvent mask routine.

Powder X-ray diffraction was measured using a Rigaku Oxford Diffraction SuperNova Dual Wavelength single crystal X-ray diffractometer using Cu-Kα radiation at 130 K. Samples were loaded into a 5mm glass capillary for measurement and data was collected to $2\theta = 60°$ with an exposure time of 60 seconds per frame.

Magnetic measurements

The dc magnetic measurements were measured with a Quantum Design Magnetic Properties Measurement System (MPMS) instrument, in an applied dc field of 1,000 Oe. The ac measurements employed a Quantum Design Physical Properties Measurement System (PPMS) with an ac susceptometer insert. The ac susceptibility measurements denoted as "zero-field" were measured in a small dc field of 0.085 Oe. The powder samples were prepared in gelatin capsules and the anisotropic Dy-containing samples were restrained using eicosane. The long moment was corrected for the eicosane and gel cap contribution and the magnetic susceptibility of the Dy-containing samples were corrected for the diamagnetic component using Pascal's constants.

Spectroscopic measurements

Diffuse reflectance UV-Vis spectra were measured on samples diluted ~5% in KBr on a Thermo Scientific Evolution 220 UV–Visible spectrophotometer. Solution state electronic absorbance spectra were measured on an Agilent Technology Cary60 UV−Visible spectrometer in dry, degassed MeCN at concentrations of 5×10^{-5} M. Fourier transform infrared spectra were measured as KBr disc on a Bruker Tensor 27 FTIR spectrometer and normalised as absorbance spectra. X-band EPR was performed on a Bruker Elexys E500 spectrometer on powder sample at room temperature. The microwave frequency used for EPR was of frequency 9.8669 GHz, with a modulation amplitude of 1.00 Gauss, microwave power of 0.200 mW and field sweep of 400 Gauss. The EPR spectrum was fit using the Easyspin

program.[61] All ^{1}H NMR spectra were acquired on a Varian MR400 400 MHz spectrometer and referenced to residual protic solvent.

Electrochemical measurements

Cyclic and rotating disk electrode voltammetry and were conducted using a standard three-electrode cell configuration under a N_2 atmosphere, with 1 mm or 3 mm diameter glassy-carbon working electrode, respectively, a Pt-wire auxiliary electrode and a leak-free Ag/AgCl reference electrode calibrated against the ferrocene/ferrocenium couple. Measurements for **2-RE** were performed with a sample concentration of 5×10^{-4} M in MeCN with 0.25 M Bu_4NPF_6 as the supporting electrolyte, while measurements for **3-Dy** employed a concentration of approximately 5×10^{-4} M in MeCN with 0.1 M Bu_4NPF_6 as the supporting electrolyte. The considerable air-sensitivity of **3-Dy** made it impossible to obtain an RDE voltammogram with our bench-top apparatus prior to significant oxidation and decomposition.

Other measurements

Elemental analyses (CHN) were performed at the Campbell Microanalytical Laboratory, University of Otago. Thermogravimetric analyses were performed on a Mettler Toledo thermal analyser using a ramp rate of 5 ºC per minute up to a maximum temperature of 400 ºC and a N_2 atmosphere.

Acknowledgements

We thank the Australian Research Council for financial support (DP170100034) to CB, KSM and RAM. MAD thanks AINSE for an AINSE Post-Graduate Research Award. This research was undertaken in part using the PPMS at the Australian Centre for Neutron Scattering and the MX1 and MX2 beamlines at the Australian Synchrotron (using the Australian Cancer Research Foundation (ACRF) detector), both part of ANSTO.

Notes and references

[a] *School of Chemistry, University of Melbourne, Melbourne, 3010, Victoria, Australia. E-mail:* c.boskovic@unimelb.edu.au

[b] *School of Chemistry, Monash University, Clayton, Victoria, 3800, Australia*

[c] *Australian Centre for Neutron Scattering, Australian Nuclear Science and Technology Organisation, Locked Bag 2001, Kirrawee DC New South Wales 2232, Australia*

† Electronic Supplementary Information (ESI) available: additional structural representations, magnetic data, powder X-ray diffracograms, thermogravimetric analysis, voltammetric data, and infrared, electronic and EPR spectra. CCDC reference numbers 1905961-1905964. For ESI and crystallographic data in CIF or other electronic format see DOI: 10.1039/b000000x/

References

1 N. Ishikawa, M. Sugita, T. Ishikawa, S.-Y.-Y. Koshihara and Y. Kaizu, *J. Am. Chem. Soc.*, 2003, **125**, 8694–5.

2 L. Sorace, C. Benelli and D. Gatteschi, *Chem. Soc. Rev.*, 2011, **40**, 3092–3104.

3 D. N. Woodruff, R. E. P. Winpenny and R. A. Layfield, *Chem. Rev.*, 2013, **113**, 5110–5148.

4 S. T. Liddle and J. van Slageren, *Chem. Soc. Rev.*, 2015, **44**, 6655–6669.

5 S. G. McAdams, A. M. Ariciu, A. K. Kostopoulos, J. P. S. Walsh and F. Tuna, *Coord. Chem. Rev.*, 2017, **346**, 216–239.

6 J.-L. Liu, Y.-C. Chen and M.-L. Tong, *Chem. Soc. Rev.*, 2018, **47**, 2431–2453.

7 F. S. Guo, B. M. Day, Y. C. Chen, M. L. Tong, A. Mansikkamäki and R. A. Layfield, *Angew. Chem. Int. Ed.*, 2017, **56**, 11445–11449.

8 C. A. P. Goodwin, F. Ortu, D. Reta, N. F. Chilton and D. P. Mills, *Nature*, 2017, **548**, 439–442.

9 F. Guo, B. M. Day, Y. Chen, M. Tong, A. Mansikkamäki and R. A. Layfield, *Science*, 2018, **362**, 1400–1403.

10 K. R. McClain, C. A. Gould, K. Chakarawet, S. Teat, T. J. Groshens, J. R. Long and B. G. Harvey, *Chem. Sci.*, 2018, **9**, 8492–8503.

11 Y.-N. Y. Guo, G.-F. Xu, Y.-N. Y. Guo and J. Tang, *Dalton Trans.*, 2011, **40**, 9953–9963.

12 K. S. Pedersen, J. Dreiser, H. Weihe, R. Sibille, H. V. Johannesen, M. A. Sørensen, B. E. Nielsen, M. Sigrist, H. Mutka, S. Rols, J. Bendix and S. Piligkos, *Inorg. Chem.*, 2015, **54**, 7600–7606.

13 L. Escalera-Moreno, J. J. Baldoví, A. Gaita-Ariño and E. Coronado, *Chem. Sci.*, 2018, **9**, 3265–3275.

14 A. Lunghi, F. Totti, R. Sessoli and S. Sanvito, *Nat. Commun.*, 2017, **8**, 1–7.

15 L. Tesi, A. Lunghi, M. Atzori, E. Lucaccini, L. Sorace, F. Totti and R. Sessoli, *Dalton Trans.*, 2016, **45**, 16635–16643.

16 A. Lunghi, F. Totti, S. Sanvito and R. Sessoli, *Chem. Sci.*, 2017, **8**, 6051–6059.

17 E. Rousset, M. Piccardo, M.-E. Boulon, R. Gable, A. Soncini, L. Sorace and C. Boskovic, *Chem. Eur. J.*, 2018, **24**, 14768–14785.

18 J. D. Rinehart, M. Fang, W. J. Evans and J. R. Long, *J. Am. Chem. Soc.*, 2011, **133**, 14236–9.

19 J. D. Rinehart, M. Fang, W. J. Evans and J. R. Long, *Nat. Chem.*, 2011, **3**, 538–542.

20 S. Demir, M. I. Gonzalez, L. E. Darago, W. J. Evans and J. R. Long, *Nat. Commun.*, 2017, **8**, 2144.

21 S. Demir, J. M. Zadrozny, M. Nippe and J. R. Long, *J. Am. Chem. Soc.*, 2012, **134**, 18546–9.

22 B. Dolinar, S. Gómez-Coca, D. Alexandropoulos and K. R. Dunbar, *Chem. Commun.*, 2017, **53**, 2283.

23 F.-S. Guo and R. A. Layfield, *Chem. Commun.*, 2017, **53**, 3130–3133.

24 S. Kitagawa and S. Kawata, *Coord. Chem. Rev.*, 2002, **224**, 11–34.

25 S. Benmansour, I. Pérez-Herráez, C. Cerezo-Navarrete, G. López-Martínez, C. Martínez Hernández and C. J. Gómez-García, *Dalton Trans.*, 2018, **47**, 6729–6741.

26 J. Tao, H. Maruyama and O. Sato, *J. Am. Chem. Soc.*, 2006, **128**, 1790–1.

27 J. S. Miller and K. S. Min, *Angew. Chem. Int. Ed.*, 2009, **48**, 262–272.

28 B. Sarkar, D. Schweinfurth, N. Deibel and F. Weisser, *Coord. Chem. Rev.*, 2015, **293**–**294**, 250–262.

29 M. Abdus Subhan, R. Kawahata, H. Nakata, A. Fuyuhiro, T. Tsukuda and S. Kaizaki, *Inorg. Chim. Acta*, 2004, **357**, 3139–3146.

30 M. A. Dunstan, E. Rousset, M. E. Boulon, R. W. Gable, L. Sorace and C. Boskovic, *Dalton Trans.*, 2017, **46**, 13756–13767.

31 R. Ishikawa, S. Michiwaki, T. Noda, K. Katoh, M. Yamashita, K. Matsubara and S. Kawata, *Inorganics*, 2018, **6**, 7.

32 R. Ishikawa, S. Michiwaki, T. Noda, K. Katoh, M. Yamashita and S. Kawata, *Magnetochemistry*,

2019, **5**, 30–42.

33 P. Zhang, M. Perfetti, M. Kern, P. P. Hallmen, L. Ungur, S. Lenz, M. R. Ringenberg, W. Frey, H. Stoll, G. Rauhut and J. van Slageren, *Chem. Sci.*, 2018, **9**, 1221–1230.

34 D. Casanova, M. Llunell, P. Alemany, S. Alvarez, P. D. Casanova, M Llunell and S. A. Alemany, *Chem. Eur. J.*, 2005, **11**, 1479–94.

35 A. Ruiz-Martínez, D. Casanova and S. Alvarez, *Dalton Trans.*, 2008, **0**, 2583–2591.

36 M. Llunell, D. Casanova, J. Cirera, J. M. Bofill, P. Alemany, S. Alvarez, M. Pinsky and D. Avnir, *SHAPE 2.0*, Universitat de Barcelona and The Hebrew University of Jerusalem, Barcelona, 2003.

37 D. Hartley and M. J. Ware, *J. Chem. Soc. A*, 1969, 138–142.

38 D. Guo and J. K. McCusker, *Inorg. Chem.*, 2007, **46**, 3257–3274.

39 J. R. Pankhurst, N. L. Bell, M. Zegke, L. N. Platts, C. A. Lamfsus, L. Maron, L. S. Natrajan, S. Sproules, P. L. Arnold and J. B. Love, *Chem. Sci.*, 2016, **8**, 108–116.

40 J. N. Schrauben, D. Guo, J. L. McCracken and J. K. McCusker, *Inorg. Chim. Acta*, 2008, **361**, 3539–3547.

41 N. G. Connelly and W. E. Geiger, *Chem. Rev.*, 1996, **96**, 877–910.

42 S. K. Langley, D. P. Wielechowski, V. Vieru, N. F. Chilton, B. Moubaraki, B. F. Abrahams, L. F. Chibotaru and K. S. Murray, *Angew. Chem. Int. Ed.*, 2013, **52**, 12014–12019.

43 Q.-W. Li, R.-C. Wan, Y.-C. Chen, J.-L. Liu, L.-F. Wang, J.-H. Jia, N. F. Chilton and M.-L. Tong, *Chem. Commun.*, 2016, **52**, 13365–13368.

44 R. Orbach and M. Blume, *Phys. Rev. Lett.*, 1962, **8**, 478–480.

45 X. Ma, E. A. Suturina, S. De, P. Négrier, M. Rouzières, R. Clérac and P. Dechambenoit, *Angew. Chem. Int. Ed.*, 2018, **57**, 7841–7845.

46 M. Ding, G. E. Cutsail III, D. Aravena, M. Amoza, M. Rouzières, P. Dechambenoit, Y. Losovyj, M. Pink, E. Ruiz, R. Clérac and J. M. Smith, *Chem. Sci.*, 2016, **7**, 6132–6140.

47 E. Lucaccini, L. Sorace, M. Perfetti, J. P. Costes and R. Sessoli, *Chem. Commun.*, 2014, **50**, 1648–

1651.

48 D. B. G. Williams and M. Lawton, *J. Org. Chem.*, 2010, **75**, 8351–8354.

49 S. Trofimenko, *J. Am. Chem. Soc.*, 1967, **89**, 3171–3177.

50 H. A. Torrey and W. H. Hunter, *J. Am. Chem. Soc.*, 1912, **34**, 702–716.

51 H. T. Balaydin, Y. Akbaba, A. Menzek, E. Şahin and S. Göksu, *Arkivoc*, 2009, **2009**, 75–87.

52 B. F. Abrahams, A. D. Dharma, B. Dyett, T. A. Hudson, H. Maynard-Casely, C. J. Kingsbury, L. J. McCormick, R. Robson, A. L. Sutton and K. F. White, *Dalton Trans.*, 2016, **45**, 1339–1344.

53 Crysalis Pro, Rigaku Oxford Diffraction, 2015.

54 N. P. Cowieson, D. Aragao, M. Clift, D. J. Ericsson, C. Gee, S. J. Harrop, N. Mudie, S. Panjikar, J. R. Price, A. Riboldi-Tunnicliffe, R. Williamson and T. Caradoc-Davies, *J. Synchrotron Radiat.*, 2015, **22**, 187–190.

55 D. Aragão, J. Aishima, H. Cherukuvada, R. Clarken, M. Clift, N. P. Cowieson, D. J. Ericsson, C. L. Gee, S. Macedo, N. Mudie, S. Panjikar, J. R. Price, A. Riboldi-Tunnicliffe, R. Rostan, R. Williamson and T. T. Caradoc-Davies, *J. Synchrotron Radiat.*, 2018, **25**, 885–891.

56 W. Kabsch, *Acta Cryst.*, 2010, **D66**, 125–132.

57 G. M. Sheldrick, SADABS, Program for Empirical Absorption Correction of Area Detector, 1996. University of Gottingen, Germany.

58 O. V. Dolomanov, L. J. Bourhis, R. J. Gildea, J. A. K. Howard and H. Puschmann, *J. Appl. Crystallogr.*, 2009, **42**, 339–341.

59 G. M. Sheldrick, *Acta Crystallogr. Sect. A Found. Crystallogr.*, 2015, **71**, 3–8.

60 G. M. Sheldrick, *Acta Crystallogr. Sect. C Struct. Chem.*, 2015, **71**, 3–8.

61 S. Stoll and A. Schweiger, *J. Magn. Reson.*, 2006, **178**, 42–55.

TOC Entry

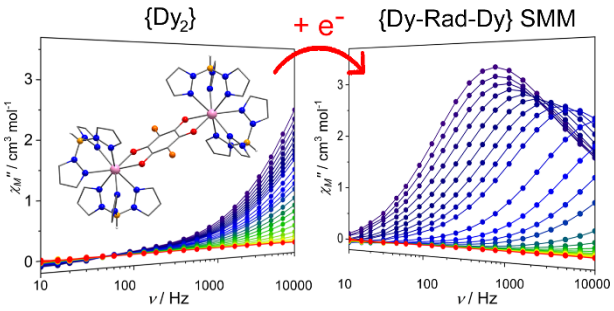

A radical bromanilate-bridged dinuclear Dy(III) complex exhibits improved single-molecule magnet performance over the parent compound with a diamagnetic bridge.